J. Membrane Biol. 32, 49–73 (1977)
© by Springer-Verlag New York Inc. 1977

Plasmalemma Transport of OH^- in *Chara corallina*

Dynamics of Activation and Deactivation

W.J. Lucas, J.M. Ferrier, and J. Dainty

Department of Botany, University of Toronto, Toronto, Ontario, Canada

Received 1 June 1976; revised 2 September 1976

Summary. The light-mediated, time-dependent rise in the pH value at the center of an alkaline band was analyzed using the methods of numerical analysis. From this analysis an expression of the time-dependent build-up of OH^- efflux was obtained for these bands. This information can now be employed to determine whether the light-activated transport of OH^- and HCO_3^- influences the electrical properties of the plasmalemma. The dark-induced deactivation of OH^- transport was also characterized, revealing a transition from efflux to a transient influx phase during deactivation.

Numerical analysis of the steady-state OH^- diffusion pattern, established along the surface of an alkaline band, revealed that the OH^- efflux width was wider than previously envisaged. It was also found that OH^- sink regions exist on either side of the efflux zone. These, and other characteristics revealed by the numerical analysis, enabled us to extend the OH^- transport model proposed by Lucas (*J. Exp. Bot.* 1975, **26**:347).

Electrophysiological studies on the Characean plasmalemma have revealed that the observed electrical properties of this membrane require the presence of an electrogenic ion transport system (Kitasato, 1968; Spanswick, 1972, 1974; Saito & Senda, 1973, 1974; Volkov, 1973; Richards & Hope, 1974). The main point of contention appears to be whether the putative H^+ transport system (Kitasato, 1968) is the sole electrogenic component, over the investigated pH range of 5.0–10.0. It is possible that when a Characean species can photosynthetically assimilate HCO_3^- the transport of this species may also be electrogenic (Walker, 1962; Hope, 1965; Volkov, 1973; Lucas, 1975*a*,*c*). However, it has been generally accepted that the OH^- ions, generated in the cytoplasm as a result of CO_2 fixation from HCO_3^- uptake, were exported across the plasmalemma on a HCO_3^-/OH^- antiporter (Lucas & Smith, 1973). A system of this nature would not have been electrogenic.

The recent finding that the HCO_3^- and OH^- transport systems function independently, the respective ions being transported across the plas-

malemma by different transporters and at spatially separate regions (Lucas, 1976), suggested that the electrical involvement of HCO_3^- and also OH^- should be further investigated. It is possible that the activation of the transport systems of these ions, at alkaline pH values, is responsible for the observed light-mediated increase in membrane conductance (Walker, 1962; Hope, 1965; Nishizaki, 1968; Spanswick, 1972; Saito & Senda, 1974).

One method of testing the involvement of HCO_3^- assimilation, in terms of its possible electrical contribution at the plasmalemma, would be to compare the time courses of photo-activated HCO_3^- and OH^- transport with the time course of membrane conductance. A close parallel between these respective time courses would be strong evidence for the electrical involvement of these ions.

The experimental difficulty is, however, in obtaining the HCO_3^- and OH^- time courses. Ideally these should be obtained on the same cell, simultaneously with the membrane potential and conductance measurements. It is impossible to obtain a $H^{14}CO_3^-$ uptake time course from a single cell, but, since OH^- efflux only occurs during HCO_3^- uptake, it may suffice to have simply the time course for the activation of the OH^- efflux system.

The time-dependent rise in the pH value at the center of an alkaline band has been fully characterized (Lucas, 1975*c*). We had hoped that this experimental information could be analyzed using time-dependent analytical diffusion equations to elucidate the manner in which OH^- efflux activates and approaches the steady-state. However, we found that these equations are at present insoluble. Only by methods of numerical analysis have we been able to successfully analyze the experimental data. This paper presents the results of this numerical analysis in terms of the dynamics of the OH^- transport activation and deactivation processes. This analysis also revealed further operational features of this system and based on these findings, the model presented by Lucas (1975*c*) has been extended.

Materials and Methods

Culture Material

Chara corallina cells were grown in large plastic containers in solutions containing (mM): 1.0–2.0 Na^+, 0.2 K^+, 0.1–0.5 Ca^{++}, 1.0 Cl^- and approximately 2 HCO_3^-. Full details of the culture techniques and the methods used to cut experimental cells have been previously reported (Lucas, 1975*b*).

Experimental Solutions

All experimental solutions contained (mM): 1.0 NaCl, 0.2 KCl, 0.2 $CaSO_4$ and 0.5 $NaHCO_3$ and were prepared using Analar Reagent grade chemicals.

pH Measurement of the OH^- Band

The pH values along the cell surface and radially away from the cell at the OH^- band center were measured using the techniques developed by Lucas and Smith (1973, *see* especially Figs. 1 and 2) and Lucas (1975*a*). Similarly, the procedures employed in measuring the response of an alkaline band to illumination were those described by Lucas (1975*a* and *c*). The pH measurements were made using a miniature pH electrode (Microelectrodes, Inc., Model MI-405) and a Leitz micromanipulator was used to position the electrode on the *Chara* cell wall.

Details of the illumination system have been previously reported (Lucas, 1975*c*).

All experiments were performed in the following sequence:

(*i*) Cells were illuminated (10 Wm^{-2}) for 1 hr and following this period the pH pattern along the entire cell wall was mapped.

(*ii*) Of the operational OH^- bands, one was selected for detailed study. The pH electrode was located on this alkaline band center.

(*iii*) Following a one-hour dark pretreatment, the light activation of this OH^- band was followed over a 30-min period; the cellular response to darkness was then recorded.

(*iv*) Sequence (*iii*) was repeated except that the respective light and dark responses were followed for 1 hr.

(*v*) At the end of the one-hour dark period the pH electrode was moved to a position on the cell surface 4 mm to the right of the OH^- band center. After a further one-hour illumination period the pH values within the vicinity of this particular OH^- band were measured.

(*vi*) The pH electrode was then raised to a position 4 mm vertically above the OH^- band center. After consecutive one-hour dark and light treatments, the vertical pH profile onto the OH^- band center was measured.

These pH measurements gave a comprehensive picture of the experimental system, with respect to a particular OH^- band. The numerical analysis was based on these measurements.

Numerical Analysis

The numerical calculation used a Fortran program on an IBM 370/165 computer. The time-dependent diffusion of OH^-, HCO_3^- and CO_3^{2-} was calculated in a two-dimensional system; the two dimensions being the direction of the axis of the cylindrical *Chara* cell and perpendicular to this axis (*see* Fig. 1). This system was spatially divided into 100 μm sections (in each direction), each section being a cylindrical ring 100 μm wide and thick. In the axial direction, the system originated at the center of an OH^- efflux band (the center of symmetry for this system) and extended over a distance of 4 mm. The radial coordinates commenced at the cell surface and similarly extended over a distance of 4 mm.

A boundary condition of zero net flux was imposed along the plane of symmetry cutting through the center of the OH^- efflux band (perpendicular to the axial direction). The boundary conditions imposed at the extremities of the system were, in general, that the concentrations at these planes equaled those of the background medium. However,

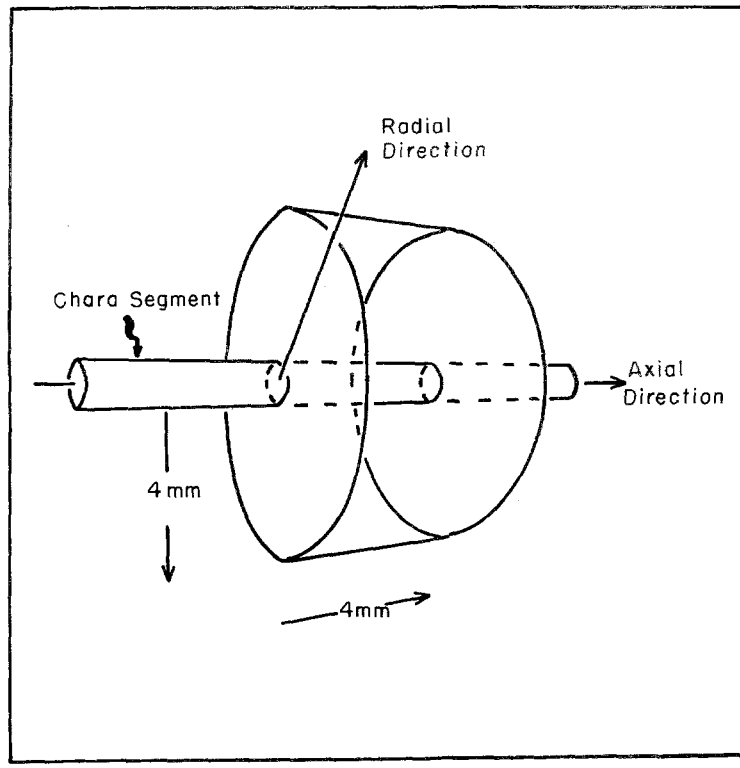

Fig. 1. Segment of *Chara* cell with boundaries of numerical diffusion region shown. One of the planes perpendicular to the axial direction of the cell cuts through the center of symmetry of the OH^- efflux band. Zero OH^- flux was the boundary condition on this plane. On the other plane, perpendicular to the axial direction, two alternative boundary conditions were used: OH^- concentration equal to the initial background concentration, or zero OH^- flux. This latter boundary condition corresponded to this plane being a plane of symmetry half-way between two OH^- efflux bands. The boundary condition on the surface 4 mm out and parallel to the cell surface was that of OH^- concentration equal to the initial background concentration

we also investigated the effect of imposing zero net flux along the plane cutting perpendicularly through the cell at a distance of 4 mm from the OH^- efflux center. (This case simulates the experimental condition of two OH^- efflux sites whose band centers are separated by a distance of 8 mm.)

To ensure stability within the calculation, it was neccessary to maintain the condition $4D\Delta t < (\Delta X)^2$, where D is the largest diffusion coefficient of the ionic species involved, Δt is the time interval used for each iteration and ΔX is the smallest spatial interval employed. For our calculations, where $\Delta X = 100$ μm and $D_{OH^-} = 2.129 \times 10^{-5}$ cm^2 sec^{-1}, a Δt value of 1 sec was employed. To verify mathematical accuracy of the calculation a limited number of runs were performed using smaller values of ΔX and Δt. In order to minimize computing time these checks were performed assuming symmetry in the axial direction. The agreement between the results obtained using $\Delta X = 10$ μm and $\Delta t = 0.01$ sec and those of the $\Delta X = 100$ μm, $\Delta t = 1$ sec case, was within 5%. For the case of $\Delta X = 50$ μm,

$\Delta t = 1$ sec, the agreement was within 3%. Because of the computing expense involved (cost increased inversely with $(\Delta X)^2$ and Δt), we were forced to accept, for the results presented in this paper, the 95% accuracy limits imposed by employing $\Delta X = 100$ μm, $\Delta t = 1$ sec. It should be stressed that we feel these limits do not detract from the predictive nature of this analysis.

Since HCO_3^- is a fundamental requirement for OH^- efflux (Lucas & Smith, 1973) all OH^- efflux experiments had to be performed in the presence of $NaHCO_3$. This meant that the chemical reaction

$$HCO_3^- + OH^- \rightleftharpoons H_2O + CO_3^{2-}$$

would occur within the immediate vicinity of the alkaline band. Hence we had to incorporate into the numerical analysis not only the diffusion of OH^- away from the efflux site but also the associated diffusion of HCO_3^- and CO_3^{2-}. To solve this system numerically it was necessary to make the basic assumption that chemical equilibrium was established in each section, following every iteration. [This appeared to be a valid assumption since the above reaction is almost instantaneous (Sirs, 1958).] Again, the added computing cost associated with the incorporation of this HCO_3^- buffering effect, forced us to do the majority of the calculations on the "simple unbuffered" system. However, sufficient cross-checks were made to ensure that the same general time-dependent diffusion pattern existed in both cases.

OH^- Efflux Activation Time Course

Initial attempts to fit the experimental pH data, associated with the light-mediated activation of the OH^- efflux band, involved calculating the time-dependent diffusion pattern using various "trial functions" for the activation of the plasmalemma transport rate. The experimental steady-state OH^- efflux value obtained using the spherical analysis technique employed by Lucas (1975*a*) gave the rate in units of moles sec^{-1}. Performing a similar cylindrical analysis on data from measurements close to the cell surface gave an equivalent rate in moles sec^{-1} per unit cell length. Hence, division of the spherical rate by the cylindrical value gave an estimate of the OH^- band pumping width. This width, along with the experimentally deduced steady-state plasmalemma efflux rate (moles cm^{-2} sec^{-1}), was used to define the required steady-state conditions in the numerical calculation.

The "trial function" that gave the best fit between experimental and numerical data was that of an exponential build-up of OH^- efflux (*see* Fig. 4). This "trial function" was rather limited, however, so the procedure was refined. The experimental pH values (60-sec intervals) were put into the program and used as "target" values. The difference between diffusion away from the central section of the OH^- band and the plasmalemma efflux rate was compared with the rate of OH^- build-up that was required to meet the next "target" pH value. This was done every second, and the plasmalemma transport rate adjusted accordingly. This procedure resulted in a fairly smooth, second by second, time curve for the efflux rate which produced a build-up (or decline) of pH at the cell surface in exact conformity with the experimental values (further details are given in the Appendix).

A similar procedure was developed for ensuring that the calculated pH values along the cell surface conformed with those obtained experimentally.

Complete details of the computational procedures associated with this OH^- efflux analysis are available from the authors.

Results

Spherical and Cylindrical Diffusion Analysis

It was essential to verify that the two-dimensional OH^- diffusion pattern, established by the numerical analysis, was comparable to the experimentally obtained data. We used the steady-state spherical and cylindrical diffusion analysis for this purpose (Lucas, 1975*a*). In the spherical system, the steady-state OH^- concentration at any radial point (C_R) is related to the radial distance (R) by the equation,

$$C_R = K\frac{1}{R} - B \tag{1}$$

where K and B are numerical constants whose values are defined by the boundary conditions. (It should be pointed out that the value of R appearing in Eq. (1) is equal to $(R_{Chara}+r)$ where r is the vertical distance from the cell surface.)

Fig. 2 is typical of the numerical results obtained and demonstrates that there was indeed close agreement between the experimental and numerical results. This was especially so for the "unbuffered" case. The slight discrepancy observed at the highest OH^- concentrates resulted from a 0.02 pH unit difference between the one-hour light activation and vertical scan experiments. (The light activation data were employed for the numerical analysis.) The fact that the "buffered" values did not fit as well as the simple "unbuffered" OH^- system was not really surprising. The complexity of the actual experimental system is perceived when one realizes that HCO_3^- uptake is also occurring along the cell surface. Because of this simultaneous HCO_3^- uptake, it is difficult to estimate the actual concentration of HCO_3^- within the immediate system. However, the numerical results expressed in Fig. 2 suggest that the HCO_3^- "buffering" effect is of rather limited importance in this diffusion system.

As previously shown, linearity of the analysis based on the spherical diffusion system was not observed close to the cell surface (*see* Lucas, 1975*a*). We considered that within this region (0.5 mm) the diffusion system may be closer to that of a cylindrical coordinate system. The steady-state diffusion equation of a hollow cylinder can be simplified to

$$C_R = G \ln R + A \tag{2}$$

where A and G are numerical constants whose values are defined by the boundary conditions. The results of a cylindrical analysis of the

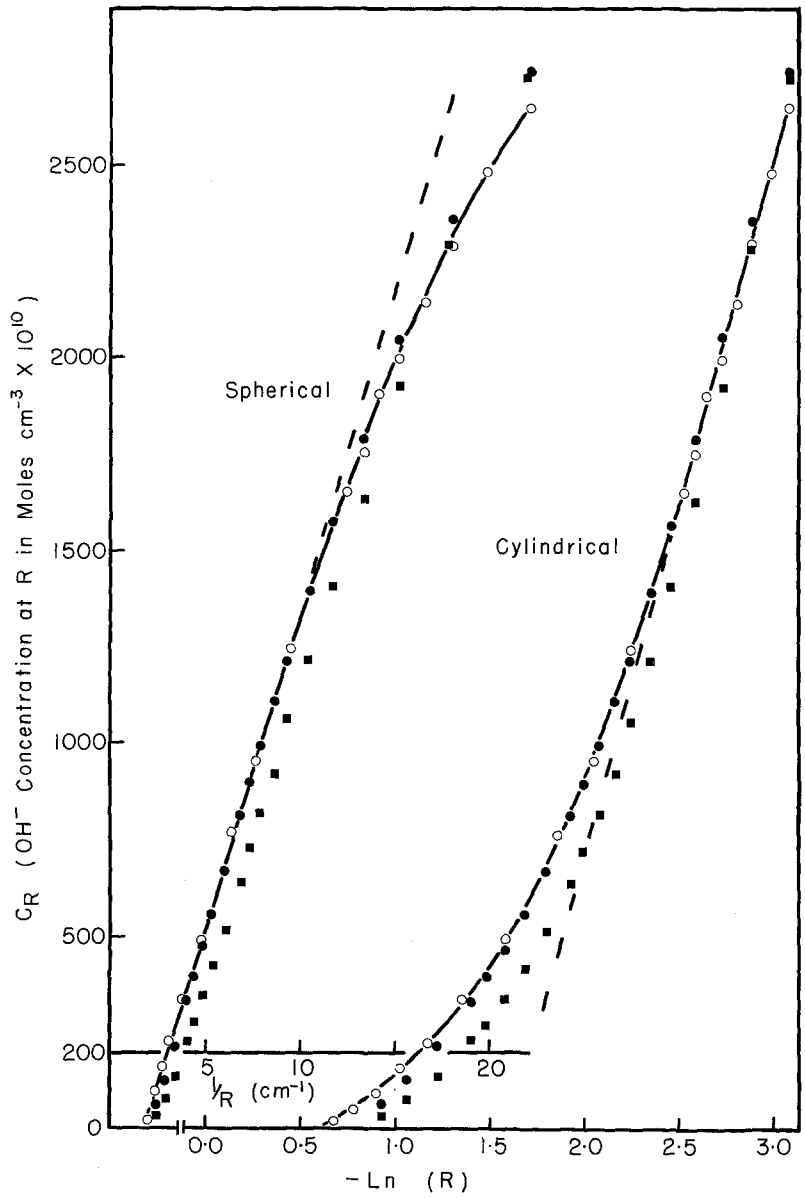

Fig. 2. Steady-state spherical and cylindrical diffusion analysis of the OH^- concentration distribution in the plane which cuts through the center of the OH^- efflux region. Symbols used: ○, experimental values; ●, calculated values; ■, calculated values with HCO_3^- buffering effect incorporated. R is the radial distance from the central axis of the cell (i.e. the cell radius plus the distance from the cell surface)

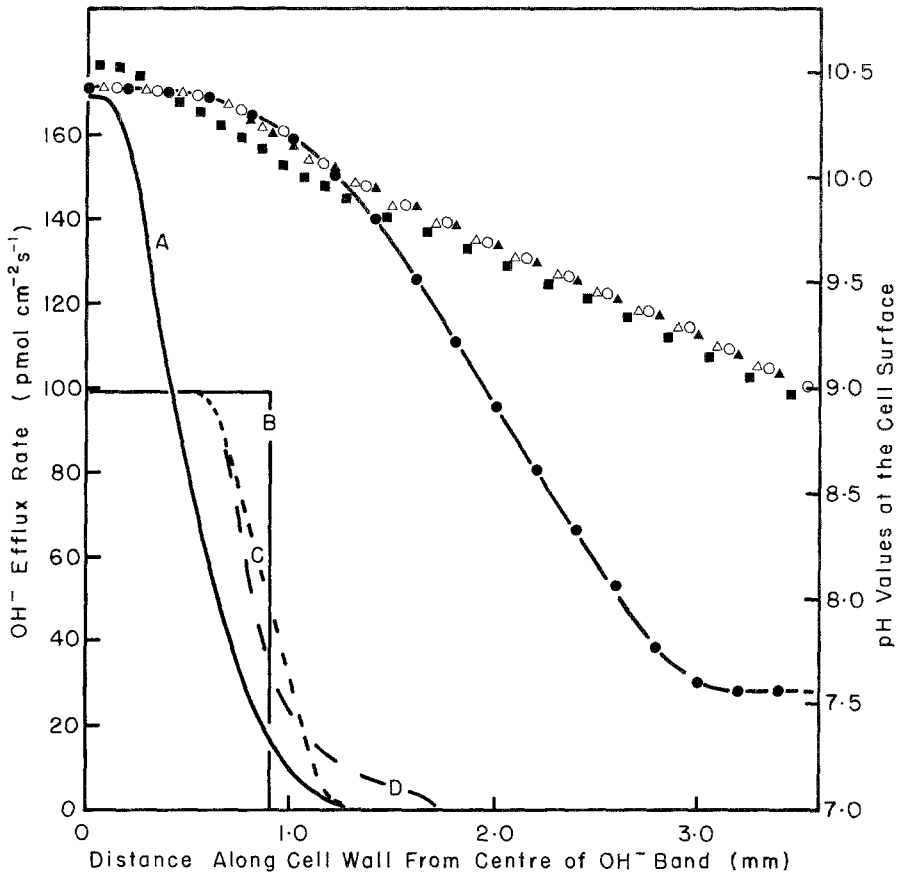

Fig. 3. Steady-state pH and OH^- efflux values along the cell surface, commencing at the efflux band center. The experimental pH values are represented by the symbol, ●. Various forms of OH^- efflux are illustrated, and the pH values calculated using the respective forms are as follows: ■, form *A* (a Gaussian distribution); △, form *B*; ○, form *C*; and ▲, form *D*

experimental and numerical values, based on Eq. (2), are presented in Fig. 2. The linear results verify our assumption concerning the OH^- diffusion pattern in the region close to the cell surface. The cylindrical analysis also revealed very close agreement between experimental and numerical results.

Some experiments were conducted over longer periods and these results showed that quasi-steady-state diffusion was established approximately 1 hr after the cell was illuminated. Again, the numerical results were in agreement with this finding.

Spatial Distribution of OH^- Efflux Activity

To obtain information relating to the actual spatial distribution of the OH^- efflux activity associated with an OH^- band, we investigated a range of efflux forms. In each case, the total OH^- efflux was the same, only the distribution of the spatial activity was varied. Fig. 3 illustrates some of the forms investigated. The Gaussian efflux distribution deviated noticeably from the observed experimental pattern. It is also apparent from Fig. 3 that the calculated pH values, for all forms investigated, deviated from the experimental data significantly as the distance from the OH^- band center increased. This feature was observed with all efflux bands studied, and its significance will be discussed in detail in a later section. At present we will confine our attention to the cell surface within 1.5 mm of the band center. From the results presented in Fig. 3, it can be seen that close agreement between experimental and numerical results was obtained with either a uniform step-function (*B*) or a uniform ramp-function (*C*). Although this analysis does not enable us to differentiate between these two generalized forms, we feel that the ramp-function is more likely to be representative of the actual OH^- efflux pattern. It should also be stressed that Fig. 3 represents only one-half of the actual OH^- efflux band, hence the total length over which OH^- was being effluxed is approximately 2.0–2.4 mm. In general, OH^- efflux widths of 1.9 to 2.2 mm were observed (*see* Table 1); this is considerably larger than the previously envisaged pumping width (Lucas & Smith, 1973; Lucas, 1975*a*).

Activation of OH^- Efflux

Fig. 4 shows the build-up of pH at the centers of two OH^- bands, as measured with the pH electrode just touching the cell surface. These data were first fitted using the "trial function" method, where it was found that the pH build-up could be closely approximated if an exponential build-up of OH^- efflux was used (*see* lower curves of Fig. 4*A* and *B*). Virtually an exact fit was obtained by using the "target pH" method, in which the difference between the efflux rate and the rate of diffusion away from the center of the efflux band was compared with the rate of build-up of OH^- required to match the observed experimental pH change. It should be emphasized that the resultant time course for the

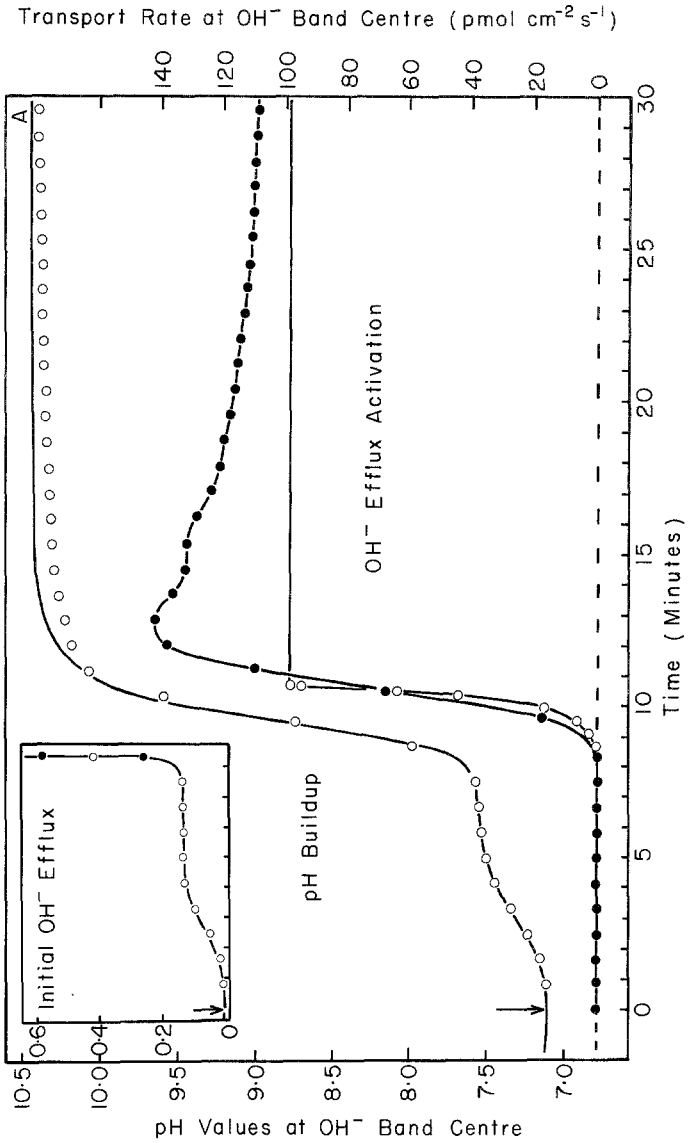

OH^- efflux build-up, obtained from this numerical procedure, is not dependent on any assumptions or parameters except the value(s) of the diffusion coefficient(s) and the background concentrations of OH^-, HCO_3^- and CO_3^{2-}.

The OH^- efflux build-up follows an exponential curve until approximately one-half of the maximum value is attained. The two general forms of OH^- efflux activation depicted in Fig. 4 are representative

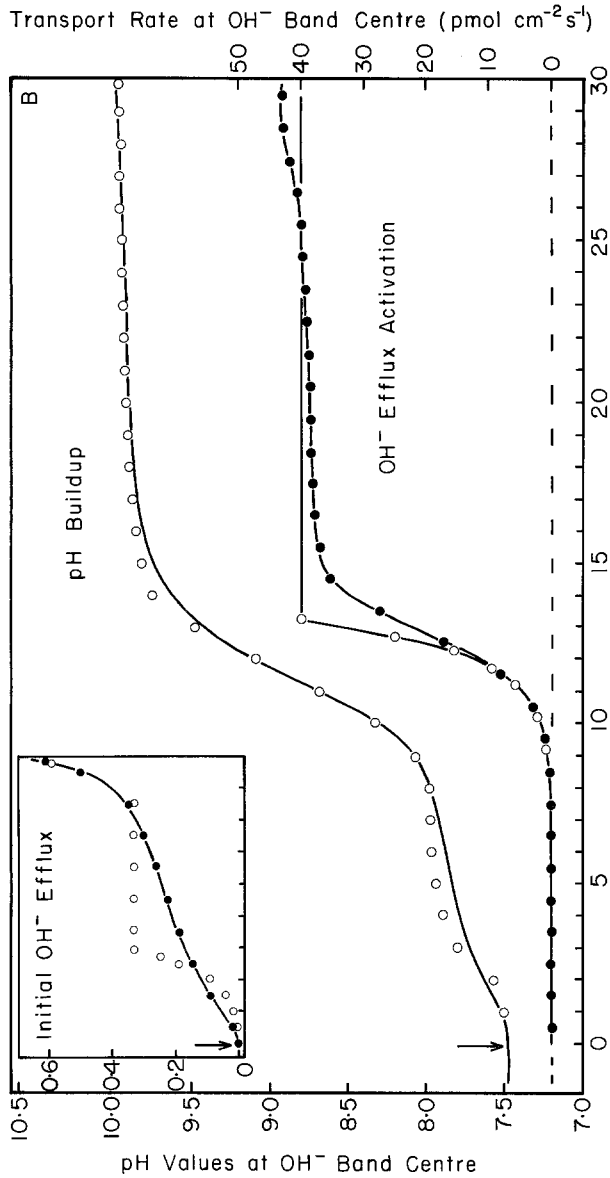

Fig. 4. pH build-up and OH^- efflux activation curves. The upper curves in *A* and *B* are experimental pH values, obtained as a function of time, at the efflux band centers. The symbol ○, associated with these pH curves, represents the numerical values obtained using exponential "trial" functions for OH^- efflux activation. The same symbol was employed, on the OH^- efflux curves, to present the exponential "trial" function OH^- efflux values. (The time constants for these exponential curves were 170 and 300 sec for *A* and *B*, respectively.) The curves associated with the solid circles (●) are the OH^- efflux activations required to give an exact fit of the respective experimental pH build-up. The inserts show, on a magnified scale, exponential (○) and "exact fit" (●) efflux activation curves for the small, initial, pH build-up. The scales on the ordinate and abscissa represent OH^- transport rate in pmole cm^{-2} sec^{-1} and time in minutes, respectively. (In *A*, these two methods gave almost the same values.) The arrows indicate the commencement of the illumination period

of the most frequently observed forms. The overshoot characteristic illustrated in Fig. 4*A* can possibly be explained using the model of Lucas (1975*c*). The reduction in efflux rate may be due to the activation of other efflux bands, which is thought to be in response to the establishment of critical activation levels of a substrate in the cytoplasm. Several cases were also observed in which the efflux rate was found to increase after activation and establishment of a quasi-steady-state. The change observed

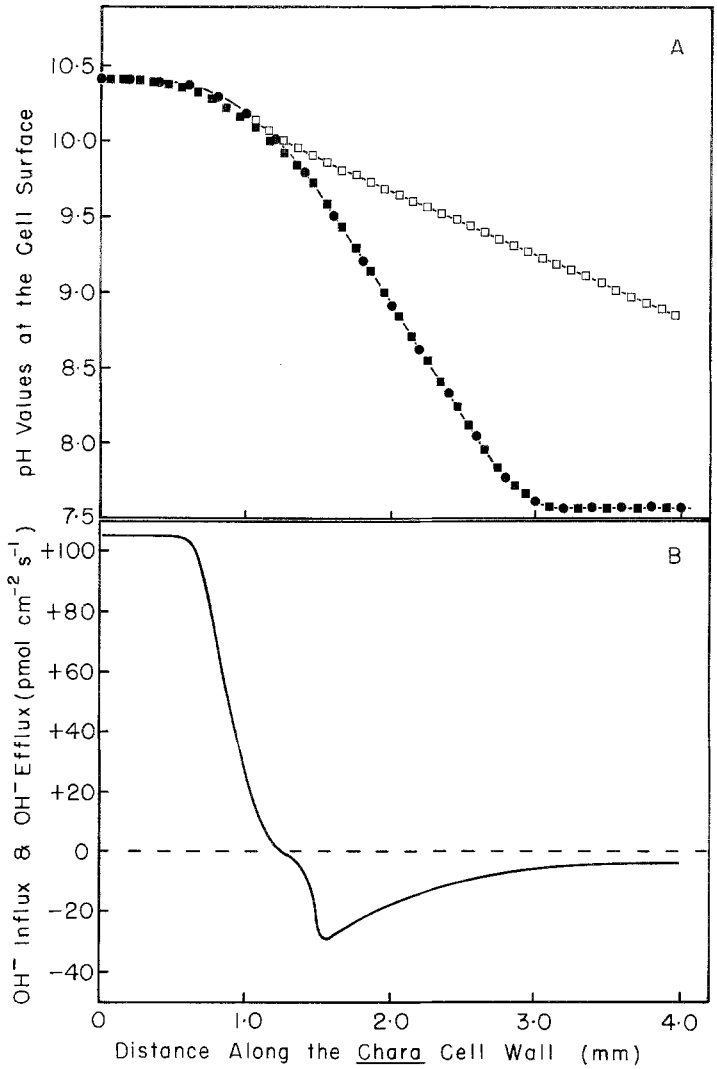

Fig. 5. Steady-state pH and OH^- efflux values along the cell surface. The solid circles (●) are experimental pH values. The solid squares (■) are pH values calculated with the OH^- efflux and sink pattern shown in the lower curve. The open squares (□) are pH values calculated with the OH^- efflux pattern shown in the lower curve, but without the lateral sink region

in the latter phase of the results presented in Fig. 4*B* is an example of this form. Hydroxyl efflux regulation, or "feedback", is in agreement with the observed OH^- efflux characteristics and models propounded by Lucas (1975*c*) and Lucas and Dainty (1976).

The inserts in Fig. 4*A* and *B* show the very small initial OH^- efflux rate which is required to produce the initial pH step that precedes the

main activation. In general, this initial efflux process fits a simple exponential form (*see* Fig. 4*A*) but as shown in Fig. 4*B*, this is not always observed. However, this small initial efflux is always present during the activation of OH^- bands in *Chara corallina*, and its possible significance as a clue to the mechanism of OH^- transport will be discussed in a later section.

Lateral OH^- Sink Requirement

When the numerical calculation was performed with zero OH^- back flux, through the cell surface adjacent to the OH^- efflux band, the experimental pH values were always substantially lower than those obtained from the numerical calculation (*see* Fig. 3 and Fig. 5*A*). To correct for this discrepancy, the computational procedure was modified so that the calculated pH values were prevented from going above their respective experimental value by incorporating an OH^- sink (influx). The strength of this sink was matched to the increase in diffusional flux, into a given section, once the respective pH value was reached. A typical band with the related OH^- efflux and sink regions is shown in Fig. 5*B*. (Since *Chara corallina* has a light-activated H^+ efflux system (Lucas & Smith, 1973), it should be realized that part of this OH^- sink may be associated with this phenomenon.)

Although the magnitude of individual sinks varied (*see* Table 1), all bands studies had OH^- sinks typified by the general shape illustrated in Fig. 5*B*. The possible significance of the lateral sink, in helping to elucidate the mechanism of OH^- transport, will be discussed later.

General Features of the OH^- Band

The numerical results presented in Table 1 were drawn from calculations performed on steady-state experimental data obtained from five OH^- bands on three cells. [These experimental data reflected typical OH^- efflux band characteristics (Lucas & Smith, 1973; Lucas, 1975*a* and *c*, 1976).] Experiments were conducted on internodal cells except for experiment 2, in which a whorl cell was used. Experiments 3, 4 and 5 were conducted on different bands on the same cell.

Some general features of the OH^- band are apparent. The width of the OH^- efflux region ranged from 1.9 to 2.2 mm. The rate of OH^-

Table 1. Steady-state hydroxyl band characteristics[a]

Computational aspects	Exp. No.	Band center pH	Efflux width (mm)	Band center efflux rate (pmol cm^{-2} sec^{-1})	Maximum lateral sink flux (pmol cm^{-2} sec^{-1})	Efflux[b] rate (pmol sec^{-1})	Lateral sink flux rate (pmol sec^{-1})	Net efflux (efflux − sink) (pmol sec^{-1})	Efflux from spherical analysis of numerical results (pmol sec^{-1})	
									OH^-	CO_3^-
$D_{OH}=2.13\times10^{-5}$ cm^2 sec^{-1}	1	10.44	2.2	105.4	29.7	5.40	1.72	3.68	5.05	
	2	9.96	1.9	42.4	7.1	1.89	0.33	1.56	1.88	
	3	10.18	2.0	64.9	26.1	2.70	0.97	1.73	2.41	
	4	10.22	2.2	66.2	18.1	3.10	0.94	2.16	2.81	
	5	10.08	2.2	49.3	21.8	2.30	0.85	1.45	2.03	
$D_{OH}=2.13\times10^{-5}$ cm^2 sec^{-1}	1	10.44	2.2	157.1	40.4	8.04	2.40	5.64	4.43	2.92
HCO_3^- buffering	2	9.96	1.9	79.5	11.6	3.54	0.59	2.95	1.63	1.84
$D_{OH}=5.32\times10^{-5}$ cm^2 sec^{-1}	1	10.44	2.2	262.5	75.4	13.42	4.46	8.96	12.18 (4.87)[c]	
	2	9.96	1.9	105.9	17.9	4.72	0.84	3.88	4.58 (1.84)[c]	
$D_{OH}=5.32\times10^{-5}$ cm^2 sec^{-1} HCO_3^- buffering	1	10.44	2.2	315.2	111.2	16.14	5.54	10.60	11.63 (4.65)[c]	3.08

[a] The values presented in this Table were obtained by numerical analysis of the experimental data, using the "target" pH method of analysis

[b] Each OH^- efflux band was divided into a number of 100 μm efflux units. The efflux rate was obtained by summation of the rates associated with these units.

[c] Efflux calculated assuming $D_{OH}=2.13\times10^{-5}$ cm^2 sec^{-1}.

uptake by the lateral sink was approximately one-third of the rate of OH^- efflux for internodal cell bands. For the single whorl cell investigated, the uptake rate was about one-sixth the efflux rate.

The effect of including HCO_3^- buffering in the calculation was to increase the efflux and lateral sink rates by almost the same factor (Experiment 1, efflux increased by 1.49×, lateral sink by 1.40×; Experiment 2, efflux increased by 1.87×, lateral sink by 1.79×). The OH^- efflux calculated from the steady-state spherical diffusion analysis was slightly reduced. However, under these conditions there was a significant movement of alkalinity in the form of CO_3^{2-}.

Because of the presence of the lateral sink, net OH^- efflux was always smaller than that from the efflux region. For the unbuffered situation it can be seen that the value obtained from the spherical analysis was always larger than that of net efflux, but smaller than from the efflux region. In the buffering calculations the situation was different, the value obtained for OH^- efflux by spherical analysis was in fact smaller than the net efflux. However, we consider that the buffering influence in the numerical calculation is probably greater than exists in the experimental situation. It is possible that the true buffering level is near the "flux cross-over point", namely where the net OH^- efflux value is equivalent to that calculated on the basis of the spherical analysis. This would be consistent with the earlier work of Lucas (1975*a*), where a close correlation was observed between $H^{14}CO_3^-$ uptake and OH^- efflux (spherical analysis).

The diffusion coefficient most frequently used for OH^- was 2.129×10^{-5} cm^2 sec^{-1} and is the limiting diffusion coefficient for NaOH. This value was used by Lucas (1975*a*) in his steady-state spherical diffusion analysis. The value was obtained using the limiting ionic conductances for Na^+ and OH^- in the Nernst-Hartley relationship (Robinson & Stokes, 1965, pp. 286–288, 465). However, since in these experiments the concentration of OH^- was considerably lower than that of Na^+, it is possible that the correct relation between conductivity and the diffusion coefficient is that of Onsager for the case of self- or tracer-diffusion (Onsager, 1945). This relationship becomes the Nernst-Einstein relation for low total concentrations. If this relation held for the experimental situation, the OH^- diffusion coefficient would be increased by a factor of 2.5 above that of the limiting NaOH case. The value for CO_3^{2-} would be increased by 1.6, while that for HCO_3^- would be decreased by 0.95. (We also theoretically investigated the possibility that there were no cations accompanying the OH^- diffusion, finding a negligible effect on

the Onsager self-diffusion relation. We similarly found that the HCO_3^- and CO_3^{2-} fluxes would have a negligible effect on the OH^- diffusion.)

Using the modified diffusion coefficient in the unbuffered calculations increased the values of OH^- efflux and sink flux by the same factor as the diffusion coefficient was increased. In the buffering calculation these two fluxes were also increased, but to a lesser extent than the increase in the value of the diffusion coefficient. The OH^- efflux which one could calculate from the steady-state spherical diffusion analysis of this buffered data, was almost the same as that obtained in the calculation with the NaOH diffusion coefficient, provided that the NaOH diffusion coefficient was used in the analysis. Of course if the modified coefficient was used, the result would be much larger.

It is important to note that the only assumptions or parameters in the numerical diffusion calculation are those concerning the HCO_3^- buffering and the diffusion coefficients. Hence, since the essential features of the OH^- bands were insensitive to the level of HCO_3^- buffering and the absolute value of the diffusion coefficient, we consider the existence of the lateral OH^- sink region to be as firmly established as the existence of the OH^- efflux region.

Dynamics of OH^- Transport Deactivation

The photosynthetic assimilation of HCO_3^- is totally light dependent and consequently, following the initiation of a dark period, the pH value at the OH^- band center begins to decline (Fig. 6 and *also see* Lucas, 1975*c*). Previously it was not possible to obtain further information from the dark pH time course, because of the complexity of the time-dependent diffusion system. However, with the aid of numerical analysis, a complete characterization of the OH^- transport deactivation process was possible.

Fig. 6*A* illustrates that even with the incorporation of the HCO_3^- buffering effect, the continued operation of the lateral OH^- sink in the dark, and an increase in the respective diffusion coefficients, it was not possible to obtain results that even approximated to the shape of the experimental pH time course. The influence of an OH^- influx (sink), of various magnitudes, activated simultaneously with the light off event, is illustrated in Fig. 6*A*. This revealed that a pH decline having at least some general characteristics in common with the experimental system, could be obtained using a dark sink flux somewhere between 10 and

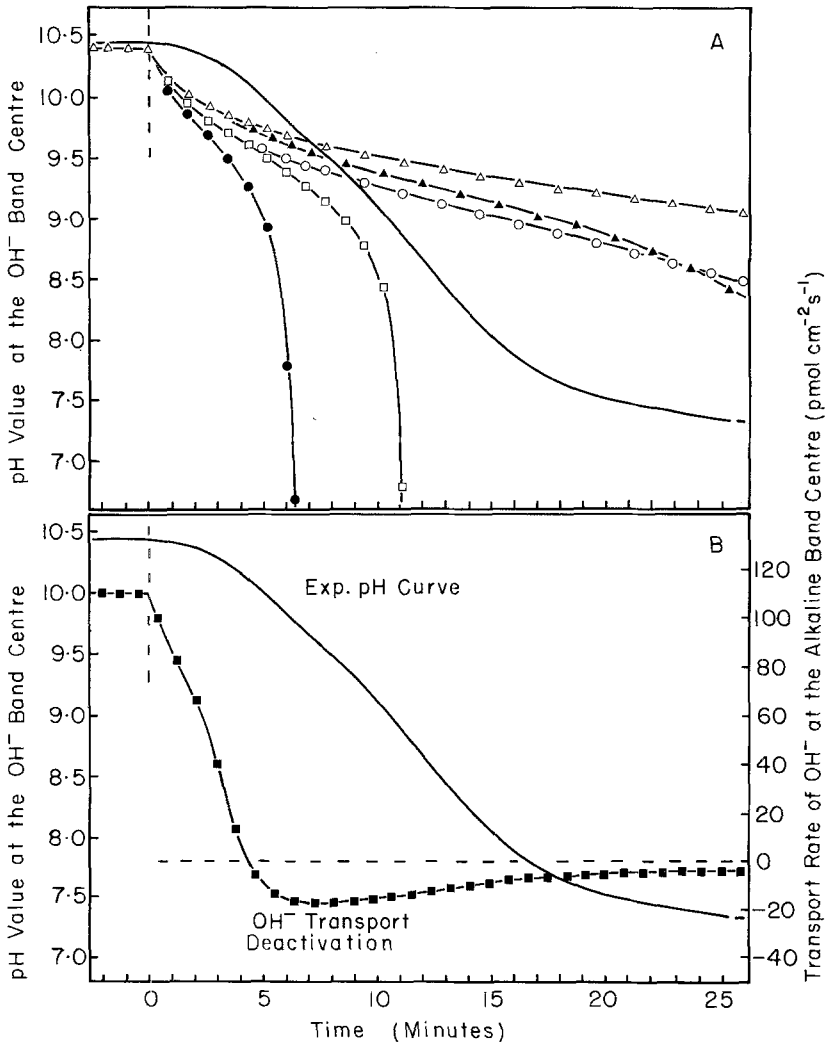

Fig. 6. Hydroxyl transport deactivation curves. The unbroken line in *A* and *B* represents the experimentally observed pH decay associated with experiment 1. The pH values were measured with the electrode on the cell surface at the OH^- band center. The other curves in *A* show calculated pH decay curves obtained for various conditions. With OH^- transport switched off at time zero, almost identical results were obtained under a range of conditions, which included the presence and absence of both a lateral sink and HCO_3^- buffering. (The lateral sink employed was equivalent to that established in the steady-state during illumination.) The results from these calculations are represented by the symbol, △. The influence of doubling the diffusion coefficient for OH^-, in the presence of a lateral sink, is also shown (○). Calculations were also done in which OH^- transport was switched to a constant influx upon cessation of illumination (these calculations also incorporated the influence of a lateral sink). A range of dark sink fluxes was investigated: ▲, 2.5 pmol cm^{-2} sec^{-1}; □, 10 pmol cm^{-2} sec^{-1}; ●, 20 pmol cm^{-2} sec^{-1}. Fig. 6*B* presents the actual OH^- transport (■), at the band center, required to generate a pH decay curve identical to the experimental case. The vertical broken line indicates the light to dark transition

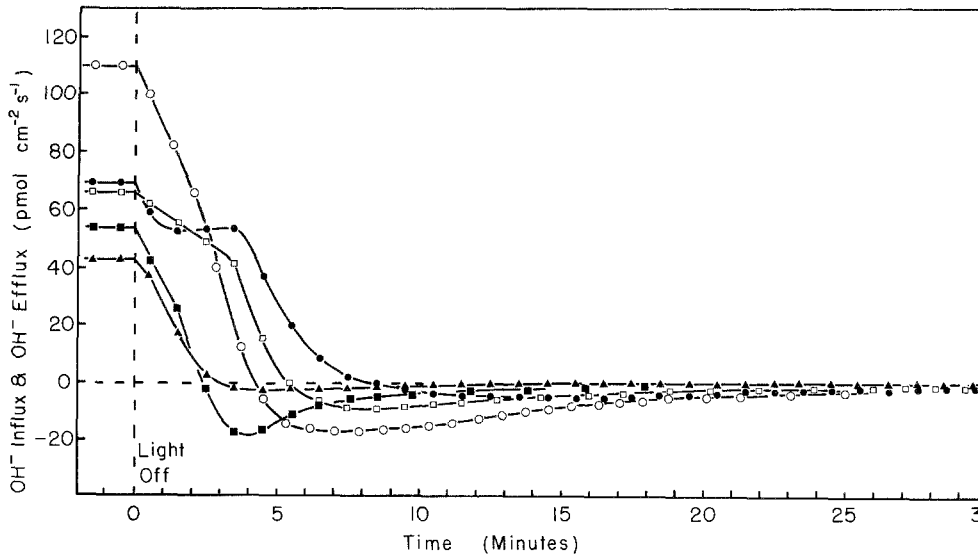

Fig. 7. Dark deactivation of OH^- transport. This Figure presents the dark deactivation results of the experiments detailed in Table 1. The individual characteristics of these curves were elucidated using the "target" calculation method. The symbols ○, ▲, □, ● and ■ represent experiments 1 through 5, respectively

20 pmole cm^{-2} sec^{-1}. However, in all the numerical results obtained for the various conditions, it can be seen that in the initial dark phase, the numerical values always fell below the experimental time course (Fig. 6*A*). This indicates that the OH^- efflux system does not deactivate immediately upon darkening.

To obtain the best estimate of the time-dependent change in OH^- transport, following the dark treatment, we employed the "target pH" method that was used to characterize the OH^- transport activation phenomenon. The results obtained using this procedure are presented in Fig. 6*B*. Following the commencement of the dark period, the OH^- efflux rate declined with what appeared to be a biphasic response. After 5 min the rate had fallen to zero efflux and, as can be seen in Fig. 6*B*, the cell surface then began to function as an OH^- sink. These general features are supported by the results presented in Fig. 7. Apparently the dark OH^- sink flux commences somewhere between 2 and 10 min after the cell is darkened, and is reduced to a very low level within a period of 30 min.

Numerical calculations were also performed to investigate the possible effect of the HCO_3^- "buffer" on the shape of the time course of OH^-

transport deactivation. Incorporation of the "buffering" effect did not change the general characteristics of the deactivation process, it merely increased the required strength of the dark sink flux. Similar results were obtained when the numerical calculations were performed using the larger OH^- diffusion coefficient. We are therefore confident that the dark OH^- deactivation phenomenon, as revealed by numerical analysis, is a realistic representation of the time course of events that actually occur in these *Chara* cells.

Discussion

The results presented above may be summarized as follows. Numerical analysis of the experimental pH data, obtained on cells of *Chara corallina,* has revealed certain important operational characteristics of the plasmalemma OH^- transport system. The initial exponential nature of the OH^- activation curve is an important discovery, for it must surely be a physical expression of a fundamental characteristic of at least one component of the OH^- transport system. A comprehensive OH^- transport "model" must incorporate this exponential phase and also explain its limited duration. We have not, as yet, formulated such a sophisticated description of the system. However, in terms of elucidating the possible electrical contribution of OH^- and HCO_3^- transport at the plasmalemma, this exponential characteristic will be an extremely useful marker.

The presence of a relatively wide, uniform OH^- efflux region and the probable ramp decline in efflux at the boundaries is of interest with respect to the recent finding by Lucas and Dainty (1977) that the OH^- transporters are uniformly distributed over the plasmalemma surface. Lucas and Dainty (1977) showed that at any one time, only a small fraction of the total number of transporters are operational. The cellular mechanism that determines the OH^- band location may also determine the density of operational transporters as a function of distance from the center of the band. If, on a molecular scale, the release of OH^- at the outer surface of the plasmalemma takes place at specific localized "enzymic transport sites", it may be possible to identify these sites and their spatial distribution using electron microscopy.

There are several possible explanations that may account for the OH^- sink in the lateral regions adjacent to the OH^- efflux zone. It may be that in this region a pH-energized transport system is operating. To function as an OH^- sink would require either the movement of OH^- into, or H^+ out of the cell. The only active transport system

proposed for this cell that involves the coupled movement of OH^- is the Cl^-/OH^- antiporter of Smith (1970). However, this system would operate in the reverse direction to that required. [In addition, this hypothesis has received only limited experimental support (Lucas & Smith, 1976.] A proton co-transport or antiport system may have more credence since this cell has a light-mediated H^+ efflux system. Spear, Barr and Barr (1969) proposed a simple HCl co-transport model for *Nitella clavata,* but this system has not gained experimental support (Lucas & Smith, 1976).

Part of the OH^- sink may be directly associated with the operation of the H^+ efflux system. We feel, however, that the characteristic shape of the OH^- sink, in terms of the spatial distribution of its relative strengths, suggests that any contribution from the H^+ efflux system is probably limited to the outer zone of the sink.

Another possibility is that there may be an efflux of CO_2 generated by the HCO_3^- influx to the cytoplasm. (Reaction of CO_2 with OH^- yields HCO_3^-, and in this manner the CO_2 efflux acts to remove OH^- from the region close to the cell surface.) Although analysis of the relation between CO_2 concentration at the cell surface and OH^- sink strength failed to reveal a simple relationship, a small contribution from this effect cannot be discounted. The possibility of passive OH^- diffusion into the cell in the lateral sink region is untenable, since this would involve movement against the electrochemical gradient for this ion. [Plasmalemma electrical potential difference is -180 to -190 mV (Lucas, 1975*d*); the pH difference is not great enough to balance this electrical potential difference.] A tentative hypothesis that we wish to forward is that the OH^- sink flux relates to an imperfection in the overall regulating mechanism controlling the cellular efflux of OH^-. Details of this hypothesis will be presented in the following section.

The biphasic deactivation response of the OH^- transport system may reflect the existence of a critical substrate level, in the cytoplasm, below which the transport system loses its efflux activity. Experimental support for the existence of critical activation and deactivation levels of an essential substrate in the cytoplasm has already been reported by Lucas (1975*c*). With the aid of numerical analysis it should be possible to design experiments to test this "critical substrate" hypothesis.

An Extension of the OH^- Transport Model

The control of OH^- transport at the molecular level is no doubt a complex process. However, it is possible to propose a fairly simple

model which accounts for the main features of the activation, steady-state, and deactivation of OH^- transport.

The first feature to be explained is the small flux which activates within 60 sec of illuminating the cell. (We consider that the linkage between cell illumination and this small OH^- efflux process is via the photosynthetic reactions occurring in the chloroplasts, The chloroplasts may provide energy to the transport system, or alternatively these reactions may be required to generate a compound that is essential for transport activity. This "compound" may also be involved in the establishment of OH^- efflux band centers.) The proposed model will assume that activation of the OH^- transporters occurs in such a way that they will actively transport OH^- in both directions across the plasmalemma. (We consider that the active nature of this process largely eliminates the influence of the membrane potential on the influx phase of this process.) Thus, in the presence of a higher pH value inside the cell than outside, a small net efflux would occur.

The activation of the undirected active transport will spread out along the cell surface in both directions from the band center. The mechanism which selects (or imparts) the location of the band center is unknown, but by experimentation we know that, once selected, the band center location is stable over a series of activations and deactivations.

The next step in the activation process is the initiation of the main efflux build-up, which occurs in the band center region as an exponential function of time, until the efflux is about one-half the maximum value. According to the proposed model, this efflux build-up is due to the cooperative effect of two events. Firstly, the imposition of directionality on the active transport process, and secondly the establishment of a critical concentration of a cytoplasmic substrate that is generated by photosynthesis (Lucas, 1975*c*). (It should be noted that we do not wish to specify, at this stage, OH^- *per se* or a substrate which generates OH^- at the transport site.) It is obvious that there are many ways in which directionality could be imparted to this membrane-bound transport system. One tentative proposal is that a conformational change, at the cytoplasm-plasmalemma interface, increases the binding affinity of the enzyme transport site for OH^- at this inner membrane surface. Similarly, a conformational change within the OH^- transport "complex" may increase the availability of energy (say ATP or $NADPH_2$) to the reactions associated with the efflux process. Whatever the molecular mechanism involved may be, it is clear that the activation of directionality does not extend as far along the plasmalemma surface, from the band

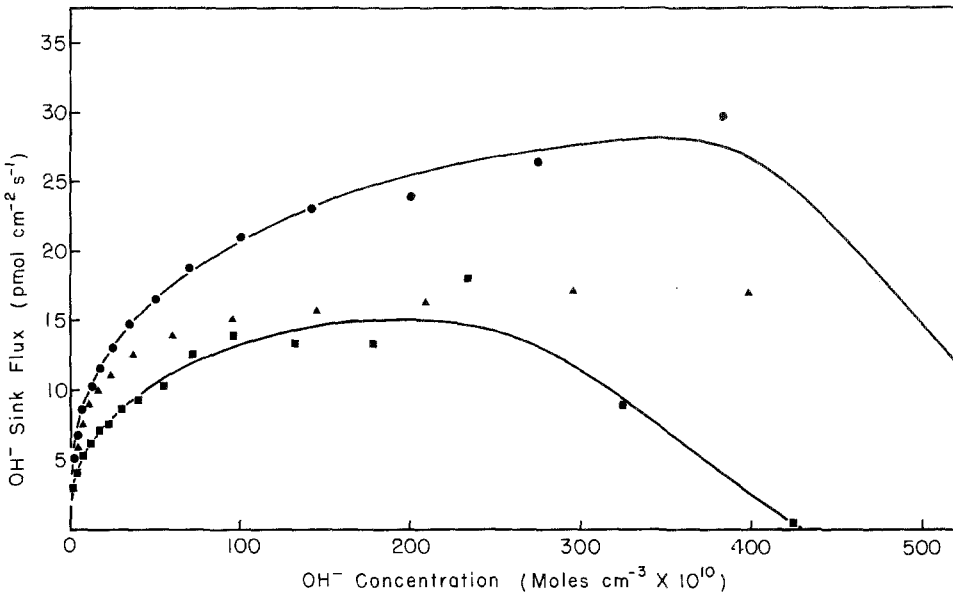

Fig. 8. Steady-state sink and dark sink flux as a function of OH^- concentration. Calculated steady-state lateral sink fluxes are plotted for experiments 1 (●) and 4 (■). Other experimental lateral sink fluxes followed similar curves. The calculated dark sink flux values (experiment 1), at the center of this OH^- band, are also given (▲). These values remained almost constant (14–17 pmole cm^{-2} sec^{-1}) for OH^- concentrations between 60×10^{-10} and 800×10^{-10} mole cm^{-3}

center, as does the activation of undirected transport. This lack of complete matching of the regions covered by the two activation processes results in the observed phenomenon of the lateral sink. That the lateral sink behaves like a simple enzymic carrier system is shown by the results presented in Fig. 8, which shows the relationship between OH^- sink flux and OH^- concentration for two OH^- bands. The influence of the directionality factor becomes apparent at higher OH^- concentrations where the sink flux falls to zero. In a similar manner, the proposed model accounts for the dark sink that is observed during the deactivation process. Photosynthetic assimilation of HCO_3^- ceases shortly after the light is turned off. Following this there is a decline in OH^- efflux, as a result of the reduction in substrate available to the transporters. A faster decay of efflux rate occurs once the directionality component is lost. The latter stage of the biphasic dark deactivation process may be an expression of the gradual loss of this directionality factor (*see* Fig. 7).

There ensues a longer period during which only the undirected transport remains. A graph of dark sink flux against OH^- concentration again follows a pattern which fits that of facilitated diffusion (Fig. 8). The concentration-limited part of the dark sink flux curve correlates closely with that of the lateral sink flux. The carrier-limited part of the dark sink flux is lower than the corresponding lateral sink flux. This can be interpreted, according to the proposed model, as indicating that the number of undirected activated transporters is decreasing in the dark case. The existence of the dark sink would thus be due to a difference in decay rate of the control process for directionality and the undirected transport, with the directionality component having the faster decay rate.

It must be emphasized that we do not claim this model as a unique solution for the observed characteristics of the OH^- transport system. We realize the limitations of this, and earlier models (Lucas, 1975*c*; Lucas & Dainty, 1977) at the molecular level. However, the successful application of numerical analysis to this OH^- efflux system now means that we are in a position to investigate the involvement of HCO_3^- and OH^- transport on the electrical properties of the plasmalemma. This study may facilitate the further refinement of the present model.

This work was supported jointly by grants from the National Research Council of Canada (Grant No. A6459) and the Connaught Fund (University of Toronto).

Appendix

Numerical Calculation of OH^- Diffusion

In the computer program, the spatial region was divided into sections designated by the subscripts i and m. The subscript i designated the annular layers concentric with the cell axis, starting with $i=1$ at the cell surface. The subscript m designated the layers that were perpendicular to the axial direction, commencing with $m=1$ at the center of symmetry of the OH^- efflux band.

The quantity $Y_i = DA_i \Delta t / \Delta x$ was first calculated, where D is the diffusion coefficient for OH^-, Δt the time interval used for each iteration, Δx the spatial size of the sections and A_i the area perpendicular to the radial direction, between section i, m and section $i+1, m$. The quantity $W_m = DB_m \Delta t / \Delta x$ was also calculated, where B_m is the area perpendicular to the axial direction between sections i, m and $i, m+1$.

The next step was to calculate $Q_{i,m}=(C_{i,m}-C_{i+1,m})\ Y_i$, where $C_{i,m}$ is the OH^- concentration in section i,m. $Q_{i,m}$ is the number of moles of OH^- moving in the radial direction from section i,m to section $i+1,m$, in time Δt. Similarly, the number of moles of OH^- moving in the axial direction ($S_{i,m}$) from section i,m to section $i,m+1$, in time Δt, was calculated using $S_{i,m}=(C_{i,m}-C_{i,m+1})\ W_m$. The number of moles of OH^- moving across the cell surface into section 1, m in time Δt, was designated $Q_{0,m}$, and was controlled by a subroutine in the program. Q and S at the other boundaries of the spatial region of the numerical calculation were controlled by other subroutines, which imposed boundary conditions closely approximating to those existing in the experimental system.

The new OH^- concentrations, in each section, were then calculated using:

$C_{i,m}=C_{i,m}+(Q_{i-1,m}-Q_{i,m}+S_{i,m-1}-S_{i,m})/V_{i,m}$, where $V_{i,m}$ is the volume of section i,m. The new values for $C_{i,m}$ were then used to calculate new Q and S values. This procedure was repeated many times, yielding the numerical approximation to the time-dependent diffusion process.

Target pH Method

Experimental pH values, obtained by placing the pH electrode on the cell surface and in the center of symmetry of an OH^- efflux band ("target pH" values), were put into the program (60-sec intervals) and converted to OH^- concentrations, CT ("target concentrations"). The change in the number of moles of OH^- in section 1,1 (at the cell surface, at the center of OH^- efflux band symmetry), in time Δt, was calculated using $R=Q_{0,1}-Q_{1,1}-S_{1,1}$, (and $S_{1,0}=0$). The change in the number of moles of OH^- in section 1,1 that should occur in Δt, if the target pH is to be matched in the calculation, is $U=(CT-C_{1,1})\ V_{1,1}/(T/\Delta t)$, where T is the time remaining until CT should be matched by $C_{1,1}$. A new value for $Q_{0,1}$ was then calculated, using $Q_{0,1}=Q_{0,1}+U-R$. This process was repeated at the beginning of every time interval (Δt) in the calculation, and was quite successful in producing a smooth sequence of calculated $C_{1,1}$ values which almost exactly matched the experimental values.

The other values of Q along the cell surface, $Q_{0,m}$, $m=2$, 3, etc., were set equal to $Q_{0,1}$ multiplied by a weighting factor. This weighting factor could be set by a subroutine which ensured that the calculated values of $C_{1,m}$ matched the measured (experimental) OH^- concentration along the cell surface.

References

Hope, A.B. 1965. Ionic relations of cells of *Chara australis*. X. Effects of bicarbonate ions on electrical properties. *Aust. J. Biol. Sci.* **18**:789

Kitasato, H. 1968. The influence of H^+ on the membrane potential and ion fluxes of *Nitella*. *J. Gen. Physiol.* **52**:60

Lucas, W.J. 1975*a*. Analysis of the diffusion symmetry developed by the alkaline and acid bands which form at the surface of *Chara corallina* cells. *J. Exp. Bot.* **26**:271

Lucas, W.J. 1975*b*. Photosynthetic fixation of ^{14}carbon by internodal cells of *Chara corallina*. *J. Exp. Bot.* **26**:331

Lucas, W.J. 1975*c*. The influence of light intensity on the activation and operation of the hydroxyl efflux system of *Chara corallina*. *J. Exp. Bot.* **26**:347

Lucas, W.J. 1975*d*. Ionic relations of *Chara corallina*: Studies on transport of HCO_3^-, OH^- and H^+ across the plasma membrane. Ph.D. Thesis. University of Adelaide, South Australia

Lucas, W.J. 1976. Plasmalemma transport of HCO_3^- and OH^- in *Chara corallina*: Non-antiporter systems. *J. Exp. Bot.* **27**:19

Lucas, W.J., Dainty, J. 1977. Spatial distribution of functional OH^- carriers along a Characean internodal cell: Determined by the effect of cytochalasin B on $H^{14}CO_3^-$ assimilation. *J. Membrane Biol.* **32**:75

Lucas, W.J., Smith, F.A. 1973. The formation of alkaline and acid regions at the surface of *Chara corallina* cells. *J. Exp. Bot.* **24**:1

Lucas, W.J., Smith, F.A. 1976. Influence of irradiance on H^+ efflux and Cl^- influx in *Chara corallina*: An investigation aimed at testing two Cl^- transport models. *Aust. J. Plant Physiol.* **3**:1

Nishizaki, Y. 1968. Light-induced changes of bioelectric potentials in *Chara*. *Plant Cell Physiol.* **9**:377

Onsager, L. 1945. Theory and problems of liquid diffusion. *Ann. N.Y. Acad. Sci.* **46**:241

Richards, J.L., Hope, A.B. 1974. The role of protons in determining membrane electrical characteristics in *Chara corallina*. *J. Membrane Biol.* **16**:121

Robinson, R.A., Stokes, R.H. 1965. Electrolyte Solutions. Second edition, Butterworths, London

Saito, K., Senda, M. 1973. The light-dependent effect of external pH on the membrane potential of *Nitella*. *Plant Cell Physiol.* **14**:147

Saito, K., Senda, M. 1974. The electrogenic ion pump revealed by the external pH effect on the membrane potential of *Nitella*. Influences of external ions and electric current on the pH effect. *Plant Cell Physiol.* **15**:1007

Sirs, J.A. 1958. Electrometric stopped flow measurements of rapid reactions in solution: Part 2. Glass electrode pH measurements. *Trans. Faraday Soc.* **54**:207

Smith, F.A. 1970. The mechanism of chloride transport in Characean cells. *New Phytol.* **69**:903

Spanswick, R.M. 1972. Evidence for an electrogenic ion pump in *Nitella translucens*. I. The effects of pH, K^+, Na^+, light and temperature on the membrane potential and resistance. *Biochim. Biophys. Acta* **288**:73

Spanswick, R.M. 1974. Evidence for an electrogenic ion pump in *Nitella translucens*. II. Control of the light-stimulated component of the membrane potential. *Biochim. Biophys. Acta* **332**:387

Spear, D.G., Barr, J.K., Barr, C.E. 1969. Localization of hydrogen ion and chloride ion fluxes in *Nitella*. *J. Gen. Physiol.* **54**:397

Volkov, G.A. 1973. Bioelectrical response of the *Nitella flexilis* cell to illumination: A new possible state of plasmalemma in a plant cell. *Biochim. Biophys. Acta* **314**:83

Walker, N.A. 1962. Effect of light on the plasmalemma of *Chara* cells. *Annu. Rep. Div. Plant Ind. C.S.I.R.O.*, p. 80